

VIP Fluorescence Turn-on Synthetic Lipid Rafts on Supramolecular Sheets and Hierarchical Concanavalin A AssemblyYongju Kim, Xin Liu, Huichang Li, and Myongsoo Lee*^[a]

Abstract: Here we report fluorescence turn-on synthetic lipid rafts by self-assembly of a cationic distyrylanthracene derivative on a negatively-charged sheet in an aqueous solution. First, the negatively-charged 2D membrane structure is formed by lateral associations of aromatic rods with carboxylate groups. Then, the synthetic rafts are floated on the surface of the negatively-charged sheets through electrostatic interactions. The fluorescence of the synthetic rafts is turned on due to the aggregation of the positively-charged AIE dye on the sheets, facilitating monitoring of the formation of rafts. Concanavalin A (Con A) protein can load hierarchically onto the synthetic rafts at neutral pH to provide discrete Con A aggregates with a uniform size of ≈ 12 nm. The uniform aggregates of Con A on the synthetic rafts can stimulate Jurkat cells with enhanced efficiency, as compared with random-sized aggregates of Con A.

Various biological systems are based on supramolecular assemblies in an aqueous solution to perform many sophisticated functions.^[1,2] One example of biological supramolecular assemblies is a protein assembly with well-defined nanostructures which can provide a powerful tool to understand specific functions such as multivalent effects in biology and biomaterial science.^[3] Another well-known example of a natural assembly is cell membranes, which are two-dimensional assembly of a lipid bilayer and proteins by cooperative noncovalent interactions.^[4–7] In cell membranes, lipid rafts are self-assembled nanodomains which have highly ordered and rigid structures through a high concentration of cholesterol and saturated fatty acids.^[4,8–10] Particularly, protein assemblies can be achieved cooperatively on the relatively rigid lipid rafts in two-dimensional lipid bilayers to provide functions in membrane signaling, apoptosis, cell adhesion and migration, protein sorting, and trafficking.^[4,9] Inspired by the features and importance of the protein assembly on lipid rafts, several kinds of research have been reported for artificial lipid rafts.^[11,12] Although the reported systems based on mostly natural components such as cholesterol, phospholipids, and fatty acids have provided a

successful strategy to in the artificial lipid rafts, it remains limitations in regard of the difficulty of direct visualization without additional dye molecules and complexity of the natural components from biological membranes.^[10,13] Therefore, construction of protein assembly on synthetic rafts with inherent fluorescence can provide a new approach for mimicking and regulating biological activities.

Synthetic supramolecules can provide a fascinating tool to form sophisticated nanostructures depending on their constituting molecular units.^[14–19] Among the building subunits for supramolecular assemblies, aromatic systems have proved to form functional supramolecular nano-architectures with dynamic fluorescence in response to external stimuli in aqueous solutions.^[20,21] For example of synthetic membranes, the lateral association of the aromatic rods in amphiphilic molecules leads into supramolecular 2D membrane structures.^[22] Aromatic macrocycles with oligoether dendron at the center of the aromatic plane self-assemble into the porous 2D structures.^[23,24] The synthetic membranes based on aromatic amphiphiles showed significant fluorescence changes in response to guests or salts through the different supramolecular interactions in aqueous solutions. Therefore, the controlled self-assembly of synthetic aromatic amphiphiles is becoming more and more a laboratory tool for sophisticated constructions of functional nanostructures.^[25–28] Here we report fluorescence turn-on synthetic rafts by the self-assembly of aggregation-induced emission (AIE) dye on negatively-charged supramolecular sheets in aqueous solution (Figure 1). The fluorescence of the synthetic rafts is turned on due to the aggregation of AIE dye on the sheets, facilitating monitoring for the formation of synthetic lipid rafts, which was limited in natural lipid rafts. The hierarchical synthetic rafts provide a stable organizing platform for discrete Con A aggregates with a uniform size which show an enhanced ability of Jurkat cell stimulation.

Amphiphile **1** was reported to self-assemble into flat sheet structures surrounded by negatively-charged carboxylates in neutral pH (Figure 1).^[29] The sheets are free standing in bulk solution with a thickness of 2.8 nm, demonstrating that the aromatic rods of **1** are packed in a monolayer arrangement in which the rods are aligned parallel to the sheet plane. Then, the aggregation behaviour of a cationic distyrylanthracene (DSA) derivative **3** with AIE property^[30] was investigated in presence of the self-assembled sheets of **1** in aqueous solution at pH 7.4. Upon addition of the dye **3** into the negatively-charged sheets of **1**, the fluorescence intensity of **3** was significantly increased, while pure **3** in pH 7.4 did not show any noticeable fluorescence emission due to an inhibition of the aggregation by electrostatic repulsions between positive charges of *N,N,N*-trimethylaniline groups of **3** (Figure 2a,b and S1). These results demonstrated that the negative charges of the

[a] Prof. Y. Kim, X. Liu, H. Li, Prof. M. Lee
State Key Lab of Supramolecular Structure and Materials
College of Chemistry, Jilin University
Changchun 130012 (China)
E-mail: msllee@jlu.edu.cn

 The ORCID identification number(s) for the author(s) of this article can be found under:
<https://doi.org/10.1002/asia.201900122>.

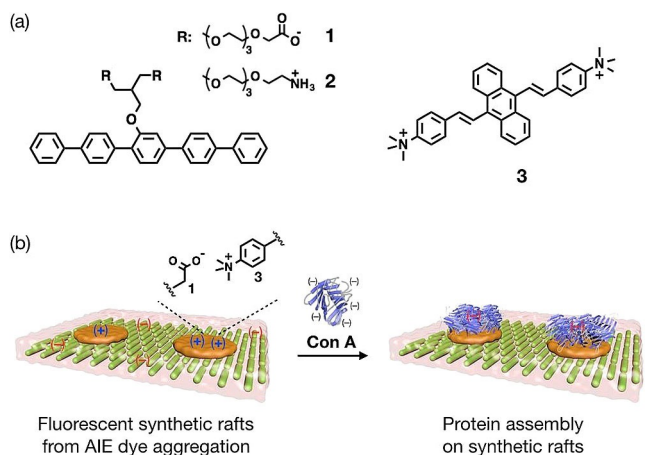


Figure 1. (a) Molecular structures of **1** and **2** for self-assembled sheets with charges, and cationic distyrylanthracene derivative **3** for fluorescent synthetic rafts. (b) Representation of aggregates of **3** for the synthetic rafts on the negatively-charged sheet of **1** through the electrostatic interaction, and hierarchical Con A assembly with uniform size on synthetic rafts. Green rods, vague pink sheets, and yellow disc represent *p*-pentaphenylene groups, negatively-charged oligoether chains, and synthetic rafts of **3**, respectively.

sheet surfaces of **1** could neutralize the positive charges of **3** to induce the aggregation of **3**. The addition of up to 0.7 equivalents of **3** into negatively-charged sheets **1** increased the fluorescence intensity (Figure 2b, inset). Zeta-potential measurements revealed that the self-assembled sheets **1** (115 μM) showed negative potential value (-55.5 ± 3.2 mV), indicating the formation of the negatively-charged surface due to the carboxylate group (Figure S2). Upon the addition of 0.7 equivalent (80.5 μM) of **3** into the sheets **1**, the zeta-potential value became -8.79 ± 0.9 mV, implying the charge neutralization between the sheets **1** and **3**.

To confirm the aggregates **3** on the sheets **1**, we performed atomic force microscopy (AFM) measurements with samples prepared by drop casting of an aqueous solution (Figure 2c and S3). In contrast to AFM image of **3** without sheets **1** (Figure S4), the image clearly revealed the micellar aggregates with 0.8 nm in height, which is consistent with the length of anthracene. Therefore, these results suggest that the anthracene groups in the aggregates are likely to be oriented perpendicular to the plane of the sheet **1**, and both ammonium groups of **3** interact with the carboxylate groups on the sur-

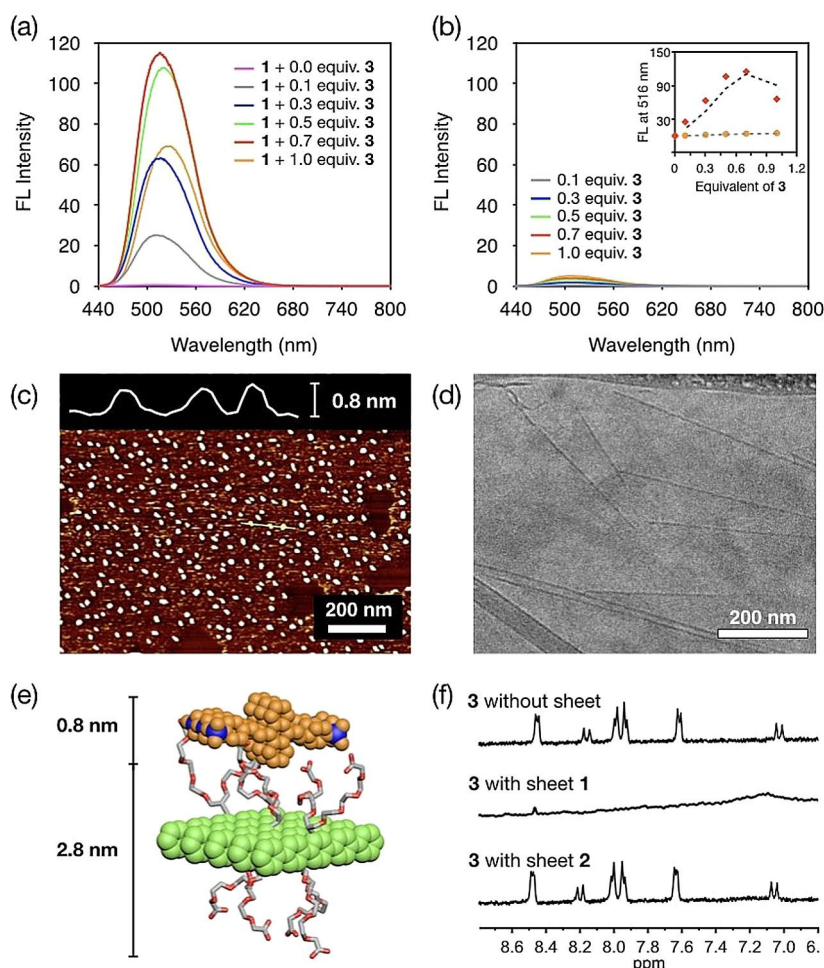


Figure 2. Emission spectra of different equivalents of **3** (a) with **1** (115 μM) and (b) without **1** in 10 mM phosphate buffer saline (PBS) solutions at 421 nm excitation wavelength. Inset is plot of fluorescence intensity at 516 nm versus the different equivalents of **3**, indicating that 0.7 equivalent of **3** provides a maximum fluorescence intensity. (c) AFM phase image of the film from evaporation of **1** (115 μM) with 0.7 equivalent of **3** in pH 7.4. The cross-sectional profile (top) is along the yellow line. (d) Cryo-TEM image of **3** in pH 7.4. (e) Schematic representation of packing arrangement of aggregate **3** on the negatively-charged sheet of **1**. (f) $^1\text{H-NMR}$ (500 MHz) spectra of **3** without and with sheets **1** and **2** in D_2O at 25 $^\circ\text{C}$.

face of the sheets **1** to decrease the electrostatic repulsions between ammonium cations (Figure 2e). Then, we performed cryogenic transmission electron microscopy (cryo-TEM) experiments with vitrified solutions. The cryo-TEM image revealed that the sheets **1** with flat structures was maintained without a collapse of their structural integrity even after the addition of **3** (Figure 2d). However, we could not observe the synthetic rafts clearly directly on sheet structures in cryo-TEM due to a limited contrast of electron density between the sheets **1** and the aggregates **3**. To observe the micellar aggregates of **3** on the sheets **1**, we performed a positively-stained TEM experiment with RuO₄ and the image showed the micellar aggregates of **3** with an average diameter of 6.7 nm (Figure S5).

This aggregation behaviour of **3** in bulk solutions was further confirmed by proton nuclear magnetic resonance (¹H-NMR) measurements (500 MHz, 25 °C). In contrast with NMR spectrum of **3** in D₂O without the sheets **1**, proton peaks associated with the aromatic units of **3** disappear in a mixture solution with the sheets **1**, indicative of the aggregation of **3** driven by the negative charges of the sheet **1** in the bulk solution (Figure 2f).^[31] To further corroborate the electrostatic interactions between carboxylates of **1** and the ammonium groups of **3** rather than intercalations of the aromatic segments of **3** into the self-assembled rods of **1**, amphiphile **2** with two amino groups at the end of flexible chains was synthesized for comparison (Figure 1a). The resulting amphiphile **2** was characterized by MALDI-TOF mass spectrometry and NMR spectroscopy to give a full agreement with the structure presented herein (Figure S6 and S7). As shown in Figure S8, amphiphile **2** also self-assembled into a flat 2D structure in an aqueous solution, demonstrating sheets surrounded by positively-charged ammonium groups at pH 7.4. The emission spectrum of **3** was not increased even after the addition of the sheet of **2** (Figure S9), and NMR spectrum of **3** with the positively-charged sheet of **2** showed the identical spectrum with **3** (Figure 2f). These results demonstrated that the aromatic segments of **3** were not intercalated into the rod segments of the sheets, but floated on the surface of the self-assembled sheets **1** through the apparent electrostatic interactions. Taken all data together, it can be considered that the fluorescence turn-on nanodomains of the positively-charged DSA dye **3** are formed by self-assembly on the negatively-charged sheet surfaces of **1** in bulk solution (Figure 1).

Inspired by the natural lipid rafts which serve as stable organizing platforms in membranes for the assembly of many functional proteins, we performed protein aggregations on the synthetic rafts in the self-assembled sheets **1**. Con A as a member of the lectin family is known for the ability to stimulate T cell subsets.^[32] The isoelectric point (pI) of Con A is in the range of 4.5–5.5, indicative of adopting negative charges in neutral pH. Because the synthetic rafts from **3** were floated on the surface of the negatively-charged sheets of **1**, one side of the rafts was considered to be exposed to the aqueous environment to provide partially positively-charged raft surfaces. Indeed, upon the addition of Con A to the synthetic rafts, the negatively-charged Con A in neutral pH showed discrete aggregates on the rafts in the sheets **1** with a quite uniform size

of about ≈ 12 nm by negatively-stained TEM image (Figure 3a). The size increase of nanodomains from 6.7 nm to 12 nm was believed to be due to an additional decrease of the electrostatic repulsions between ammonium cations of **3** by the negatively-charged Con A in pH 7.4. As shown in Figure 3b, the positively-charged sheets of **2** without the synthetic rafts demonstrated the Con A aggregates with random sizes in the range of 10 to 50 nm, indicating that synthetic rafts could play an important role in the formation of discrete Con A aggregates with a uniform size (Figure S10).

To further corroborate the interactions between the synthetic rafts and Con A, we performed fluorescence resonance energy transfer (FRET) experiments using CF555-labeled Con A. The loading of CF555-labeled Con A to the synthetic rafts on sheets **1** was expected to bring the synthetic rafts and Con A in close proximity, enabling that the energy transfer from the DSA donor of synthetic rafts to the acceptor CF555 occurs. Indeed, the addition of CF555-labeled Con A into synthetic rafts resulted in a notable appearance of an acceptor emission peak at near 580 nm, indicating that Con A effectively load on fluorescent synthetic rafts in bulk solution (Figure 3c, S11 and S12). Two-dimensional structure of the aggregated Con A on the synthetic rafts was also obtained by fluorescence optical microscopy (FOM) measurement, demonstrating that the CF555-labeled Con A was localized on the 2D sheet structures without the collapse of their 2D integrity in bulk solution (Figure 3d).

We then performed T cell stimulation experiments through Con A aggregates on the synthetic rafts (**3** on **1**) and the sheets **2**. In the cytotoxicity test, the viability values were not notably different between samples, demonstrating that self-assembled sheets with Con A are cytocompatible without sacrificing cell viability (Figure 4b). The degrees of stimulation of T cell were evaluated using ELISA assay for the measurements of induced interleukin 2 (IL-2) in Jurkat cells (human T lymphocyte). After 24 hours' incubations of Jurkat cell with free Con A and the Con A aggregates based on the synthetic rafts (**3** on **1**) and the sheets **2**, cell media were harvested and IL-2 levels in the supernatant were also measured by ELISA (Figure 4a). The assay revealed that Con A aggregates increase the release of IL-2 compared with non-aggregated Con A. Notably, the discrete Con A aggregates with a uniform size on synthetic rafts could release more IL-2 than the Con A aggregates on the sheets **2** with random size; the increases of IL-2 production were approximately 60.4% and 16.4% respectively, compared with non-aggregated Con A monomer in 100 μg mL⁻¹ of materials. These results implied that the size uniformity in the discrete Con A aggregations even under equal protein concentrations could regulate T cell activation.

In conclusion, we demonstrated that the positively-charged molecule **3** with AIE property can self-assemble into nanodomains on the negatively-charged sheets **1**, suggesting the formation of partially positively-charged synthetic rafts with strong fluorescence emission. The negatively-charged Con A proteins could load onto the positively-charged synthetic rafts at neutral pH through electrostatic interactions to provide discrete Con A aggregates with a uniform size. The uniform ag-

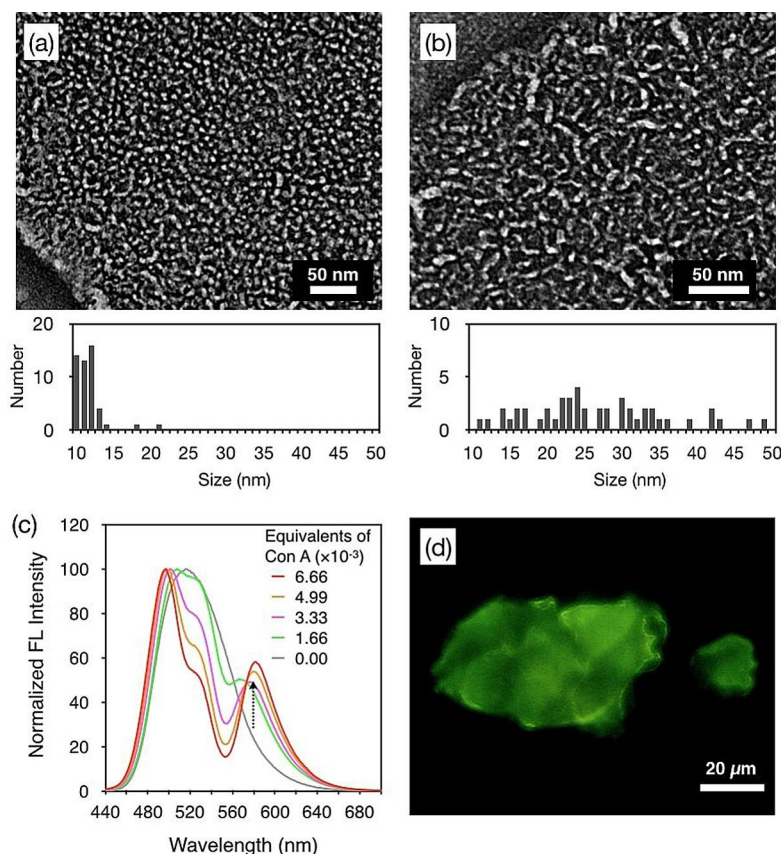


Figure 3. Negatively-stained TEM images of Con A on (a) synthetic rafts and (b) sheets of **2** in pH 7.4. The bottom shows size profiles of Con A aggregates in the range of 10 to 50 nm. (c) Emission spectra (excited at 421 nm) for FRET experiments upon the addition of CF555-labeled Con A solution to the fluorescent synthetic rafts. Equivalents of Con A is based on the synthetic rafts of **3** (80.5 μm) (d) Fluorescence optical microscopy (FOM) image of CF555-labeled Con A (12 μg) on **1** (115 μm) with 0.7 equivalent of **3** in pH 7.4 (excitation filter at 450–490 nm).

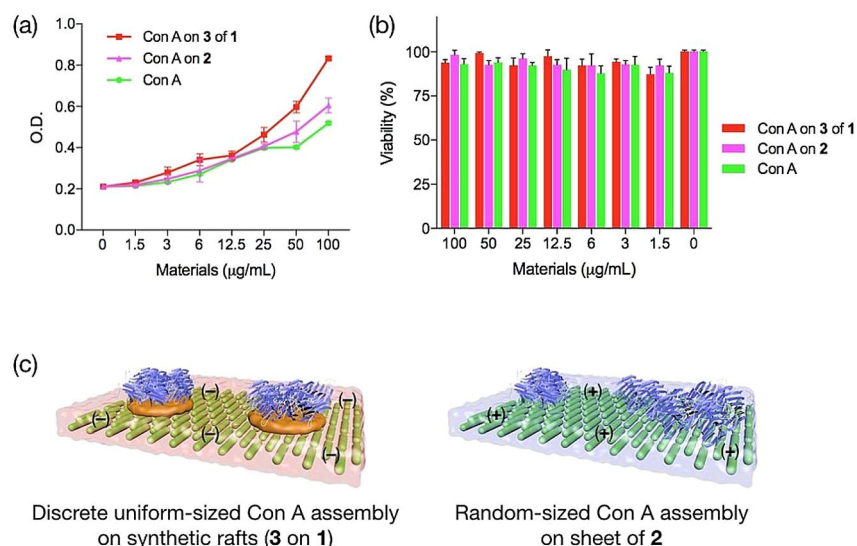


Figure 4. (a) Comparison of IL-2 production by Con A and the aggregated Con A. The error bars are based on the standard deviations from three experiments performed in duplicate, and some are smaller than the symbols. (b) The viability test using the water-soluble tetrazolium salt (WST) method of Jurkat cells grown for 48 hours with Con A samples. (c) Schematic representation of Con A aggregations on the synthetic rafts in the sheet **1** and on the sheet **2** for the stimulation of Jurkat cells.

gregates (≈ 12 nm) of Con A on the synthetic rafts of the sheet surfaces of **1** could stimulate Jurkat cells with enhanced efficiency, compared with random-sized aggregates of Con A

(10 to 50 nm) on the sheets **2**. We envisage that the incorporation of proteins in the synthetic rafts on the self-assembled sheets could provide a useful tool to control many sophisticat-

ed biological functions such as signal transductions and activations.

Experimental Section

Materials. All reactions were performed either in oven-dried glassware under dry argon atmosphere. Dichloromethane (DCM) and acetonitrile was dried by distillation from CaH₂. Distilled water was polished by ion exchange and filtration. Other solvent and organic reagent were purchased from commercial vendors and used without further purification unless otherwise mentioned. The products were purified by flash column chromatography on silica gel (230–400 mesh). Thin-layer chromatography (TLC) was performed on pre-coated glass-backed plates (silica gel 60 F₂₅₄ 0.25 mm), and components were visualized by observation under UV light (254 and 365 nm) or by treating the plates with iodine, anisaldehyde, KMnO₄, phosphomolybdic acid, and vanillin followed by heating. For biological experiments, ConA, CF[™] 555 succinimidyl ester, WST-1, BSA and Monoclonal ANTI-FLAG M2-Peroxidase (HRP) clone M2 were purchased from Sigma–Aldrich. RPMI medium 1640, fetal bovine serum and Penicillin-streptomycin were purchased from Gibco (USA). TMB solution, rabbit anti-IL-2 polyclonal antibody (ab9618), and mouse anti-IL-2 monoclonal antibody (ab38151) were purchased from abcam (UK). Cryo-preserved Jurkat cell, Clone E6–1 (human T lymphocyte) and media were purchased from Shanghai Institute of Biochemistry and Cell Biology, CAS.

Instrumentation and measurements. ¹H and ¹³C NMR spectra were obtained on 500 or 300 MHz FT-NMR spectrometer. Chemical shifts were reported in ppm relative to the residual solvent peak (CDCl₃:¹H, 7.26) or tetramethylsilane (TMS) peak. Multiplicity was indicated as follows: s (singlet), d (doublet), t (triplet). Coupling constants are reported in Hz. Matrix-Assisted Laser Desorption/Ionization Time of Flight Mass Spectrometry (MALDI-TOF-MS) was performed on a Bruker Microflex LRF20 using α -cyano-4-hydroxy cinnamic acid (CHCA) or *trans*-2-[3-(4-tertButylphenyl)-2-methyl-2-propenylidene]malononitrile (DCTB) as a matrix. The UV/Vis spectra were obtained from a Hitachi U-2900 Spectrophotometer. The fluorescence spectra were obtained from a Hitachi F-7000 fluorescence spectrophotometer. The absorbance of ELISA assay was observed from a BioTek ELx-808 plate reader. Cell were cultured at a Sanyo MCO-18AIC(UV) CO₂ incubator. Zeta-potential measurements were performed on a Zetasizer NanoZS instrument (Malvern Instruments). Fluorescence decay spectra were obtained from EDINBURGH instrument FLS920.

TEM Experiments. To investigate the self-assembled structures, a drop of each sample solution was placed on a carbon-coated copper grid (Carbon Type B (15–25 nm) on 200 mesh, with Formvar; Ted Pella, Inc.) and the solution was allowed to evaporate under ambient conditions. These samples were stained negatively by depositing a drop of uranyl acetate aqueous solution (0.2–0.4 wt%) onto the surface of the sample-loaded grid. For the positive staining, the sample-loaded grids were exposed to the RuO₄ vapor from mixture of RuCl₃·3H₂O (0.2 g) and 5% NaClO (10 mL) for 5 minutes. The dried specimen was observed by a JEOL-JEM HR2100 operated at 120 kV. The cryogenic transmission electron microscopy (cryo-TEM) experiments were performed with a thin film of aqueous solution (5 μ L) transferred to a lacey supported grid. The thin aqueous films were prepared under controlled temperature and humidity conditions (97–99%) within a custom-built environmental chamber in order to prevent evaporation of water from sample solution. The excess liquid was blotted with filter paper for 2–3 seconds, and the thin aqueous films were rapidly vit-

rified by plunging them into liquid ethane (cooled by liquid nitrogen) at its freezing point. The grid was transferred, on a Gatan 626 cryo holder, using a cryo-transfer device and transferred to the JEOL-JEM HR2100 TEM. Direct imaging was carried out at a temperature of approximately –175 °C and with a 120 kV accelerating voltage, using the images acquired with a Dual vision 300 W and SC 1000 CCD camera (Gatan, Inc.; Warrendale, PA). The data were analyzed using Digital Micrograph software.

AFM experiments. The sample films on mica surface were prepared from evaporation of sample solution. The measurements were conducted on a MultiMode 8 AFM with NanoScope V controller, NanoScope software and NanoScope Analysis software (Bruker AXS Corporation, Santa Barbara, CA, USA) in air at ambient temperature (ca. 25 °C) in the tapping mode.

CF555-Labeled ConA. 50 μ L of the 10 mM CF[™] 555 succinimidyl ester in PBS solution was added to 2 mL of ConA (2.5 mg mL⁻¹) in PBS (1.25 mM, pH 7.4) solution in a dropwise carefully. Then the mixture was stirred gently at room temperature for 1 hour. After 1 h, the samples were subjected to Sephadex G-50 column equilibrated in PBS buffer (1.25 mM, pH 7.4) to separate the labeled protein from the free dye. The concentration of the CF555-labeled ConA of the eluate from column was calculated as in PBS (1.25 mM, pH 7.4).

Fluorescence Resonance Energy Transfer Experiments (FRET). 0, 5, 10, 15 and 20 μ L of stock solutions (0.6 mg mL⁻¹, PBS 1.25 mM, pH 7.4) of CF555-labeled ConA were added to the solution (200 μ L) of sheet of **1** (115 μ m) with synthetic rafts of **3** (80.5 μ m). The samples were equilibrated for 30 min and subjected to measure the emission spectra at excitation wavelength, 421 nm.

Cell viability assay. Jurkat cells were incubated in RPMI medium 1640 with 10% fetal bovine and 100 units mL⁻¹ penicillin-streptomycin at 37 °C, 5% CO₂. The viability of Jurkat cell was investigated using the Cell cytotoxicity assay kit (water-soluble tetrazolium salt (WST) method). 100 μ L Jurkat cell (1.5 \times 10⁵ cells mL⁻¹) had been incubated for 2 days with 50 μ L materials (0, 1.5, 3, 6, 12.5, 25, 50, 100 μ g mL⁻¹ sheet + 0.7 equiv **3** + 0.14 equiv Con A) in a 96-well microplate. Then the WST-1 reagent solutions (10 μ L) were added to each well and incubated for another 4 hours at 37 °C, 5% CO₂ and subjected to plate reader to monitor the absorbance at 450 nm. The background signals were determined under the same concentration of materials without cells. The control signals were obtained from cells without materials. Viability values were calculated from the formula: (observed signal-background signal)/control signal \times 100 = viability %.

Sandwich ELISA. The amount of interleukin 2 that is released from cell was evaluated with the sandwich ELISA method. 100 μ L Jurkat cells (1.5 \times 10⁵ per mL) were incubated with pre-incubated solution at various concentrations of materials (0, 1.5, 3, 6, 12.5, 25, 50, 100 μ g mL⁻¹ sheet + 0.7 equiv **3** + 0.14 equiv Con A) at 37 °C, 5% CO₂ condition. After 24 hours of cell culture, cell media were harvested and centrifuged at 2000 rpm in an Eppendorf tube for 4 min at room temperature. The supernatant was transferred to a new tube, and the pellet was discarded. For sandwich assay, 100 μ L of sample solutions were loaded on 96 wells which were coated with 100 μ L of rabbit anti-IL-2 polyclonal antibody (5 μ g mL⁻¹). After 12 hours incubation at 4 °C, 200 μ L of 0.5% BSA solution was used for blocking, 100 μ L of mouse anti-IL-2 monoclonal antibody (5 μ g mL⁻¹) was used to form sandwich complexes. Then, 100 μ L of monoclonal anti-flag M2-peroxidase (HRP) clone M2 (5 μ g mL⁻¹) was added to react with 100 μ L of TMB (2.08 mM) solution, and 100 μ L of stopping solution (2 M H₂SO₄) was added. The absorbance of solution was measured at 450 nm using a plate reader.

Acknowledgements

This work was supported by NSFC (Grant 51473062 and Grant 21634005) and Jilin University Funding (JLUSTIRT).

Conflict of interest

The authors declare no conflict of interest.

Keywords: aggregation-induced emission · protein assembly · self-assembly · supramolecular sheets · synthetic lipid rafts

- [1] J.-M. Lehn, *Proc. Natl. Acad. Sci. USA* **2002**, *99*, 4763–4768.
- [2] D. A. Uhlenheuer, K. Petkau, L. Brunsveld, *Chem. Soc. Rev.* **2010**, *39*, 2817–2826.
- [3] Q. Luo, C. Hou, Y. Bai, R. Wang, J. Liu, *Chem. Rev.* **2016**, *116*, 13571–13632.
- [4] D. Lingwood, K. Simons, *Science* **2010**, *327*, 46–50.
- [5] S. Zhang, *Nat. Biotechnol.* **2003**, *21*, 1171–1178.
- [6] M. Klingenberg, *Nature* **1981**, *290*, 449–451.
- [7] M. Edidin, *Nat. Rev. Mol. Cell Biol.* **2003**, *4*, 414–418.
- [8] J. A. Allen, R. A. Halverson-Tamboli, M. M. Rasenick, *Nat. Rev. Neurosci.* **2007**, *8*, 128–140.
- [9] T. P. W. McMullen, R. N. A. H. Lewis, R. N. McElhaney, *Curr. Opin. Colloid Interface Sci.* **2004**, *8*, 459–468.
- [10] S. Munro, *Cell* **2003**, *115*, 377–388.
- [11] K. Gousset, N. M. Tsvetkova, J. H. Crowe, F. Tablin, *Biochim. Biophys. Acta Biomembr.* **2004**, *1660*, 7–15.
- [12] A. J. Curwin, M. A. LeBlanc, G. D. Fairn, C. R. McMaster, *PLoS ONE* **2013**, *8*, e55388.
- [13] D. Hakobyan, A. Heuer, *PLoS ONE* **2014**, *9*, e87369.
- [14] T. F. A. De Greef, M. M. J. Smulders, M. Wolffs, A. P. H. J. Schenning, R. P. Sijbesma, E. W. Meijer, *Chem. Rev.* **2009**, *109*, 5687–5754.
- [15] T. Shimizu, M. Masuda, H. Minamikawa, *Chem. Rev.* **2005**, *105*, 1401–1443.
- [16] A. Ajayaghosh, V. K. Praveen, *Acc. Chem. Res.* **2007**, *40*, 644–656.
- [17] T. Aida, E. W. Meijer, S. I. Stupp, *Science* **2012**, *335*, 813–817.
- [18] B. M. Rosen, C. J. Wilson, D. A. Wilson, M. Peterca, M. R. Imam, V. Percec, *Chem. Rev.* **2009**, *109*, 6275–6540.
- [19] X. Zhang, S. Rehm, M. M. Safont-Sempere, F. Würthner, *Nat. Chem.* **2009**, *1*, 623–629.
- [20] H.-J. Kim, T. Kim, M. Lee, *Acc. Chem. Res.* **2011**, *44*, 72–82.
- [21] Y. Kim, W. Li, S. Shin, M. Lee, *Acc. Chem. Res.* **2013**, *46*, 2888–2897.
- [22] E. Lee, J.-K. Kim, M. Lee, *Angew. Chem. Int. Ed.* **2009**, *48*, 3657–3660; *Angew. Chem.* **2009**, *121*, 3711–3714.
- [23] Y. Kim, S. Shin, T. Kim, D. Lee, C. Seok, M. Lee, *Angew. Chem. Int. Ed.* **2013**, *52*, 6426–6429; *Angew. Chem.* **2013**, *125*, 6554–6557.
- [24] B. Sun, Y. Kim, Y. Wang, H. Wang, J. Kim, X. Liu, M. Lee, *Nat. Mater.* **2018**, *17*, 599–604.
- [25] V. Percec, D. A. Wilson, P. Leowanawat, C. J. Wilson, A. D. Hughes, M. S. Kaucher, D. A. Hammer, D. H. Levine, A. J. Kim, F. S. Bates, K. P. Davis, T. P. Lodge, M. L. Klein, R. H. DeVane, E. Aqad, B. M. Rosen, A. O. Argintaru, M. J. Sienkowska, K. Rissanen, S. Nummelin, J. Ropponen, *Science* **2010**, *328*, 1009–1014.
- [26] S. Zhang, H.-J. Sun, A. D. Hughes, R.-O. Moussodia, A. Bertin, Y. Chen, D. J. Pochan, P. A. Heiney, M. L. Klein, V. Percec, *Proc. Natl. Acad. Sci. USA* **2014**, *111*, 9058–9063.
- [27] D. K. Smith, F. Diederich, *Chem. Eur. J.* **1998**, *4*, 1353–1361.
- [28] H. Jin, W. Huang, X. Zhu, Y. Zhou, D. Yan, *Chem. Soc. Rev.* **2012**, *41*, 5986–5997.
- [29] X. Liu, H. Li, Y. Kim, M. Lee, *Chem. Commun.* **2018**, *54*, 3102–3105.
- [30] X. Li, K. Ma, S. Zhu, S. Yao, Z. Liu, B. Xu, B. Yang, W. Tian, *Anal. Chem.* **2014**, *86*, 298–303.
- [31] J. Liu, J. Song, *PLoS ONE* **2009**, *4*, e7805.
- [32] J. M. Dwyer, C. Johnson, *Clin. Exp. Immunol.* **1981**, *46*, 237–249.

Manuscript received: January 23, 2019

Revised manuscript received: February 17, 2019

Accepted manuscript online: February 19, 2019

Version of record online: February 25, 2019